# Electrokinetics in Fixed Beds: Experimental Demonstration of Electroosmotic Perfusion**

Ulrich Tallarek,* Erdmann Rapp, Henk Van As, and Ernst Bayer

The concept of an intraparticle forced convection to reduce the resistance to mass transfer of a stagnant mobile phase in liquid chromatography has received considerable attention over the last decade, both from a theoretical and a particle engineering point of view.[1–9] By tuning the permeability of the porous particles to typical drops in column pressure, the actual pressure gradient in a fixed bed may act as a driving force for an intraparticle flow[10] so that an already small, but non-zero flow component assists or even dominates the slow diffusion of large molecules and reduces the hold-up dispersion that arises from stagnant zones. An important aspect in the design of particles has been the hierarchical architecture of the pore network to which several sets of pores may contribute.[1, 7, 9] The term perfusion chromatography differs from diffusion-limited operations in that it specifically refers to any separation process in which the intraparticle velocity is not zero.[2] However, a mobile-phase perfusion with pressure-driven flows may be operative only when relatively high drops in column pressure and particles with large pores (that have a low adsorptive capacity) are used. In any case, the intraparticle fluid velocity remains very small compared to the velocity in the interparticle pore space.

It has also been clearly demonstrated over the last decade that an electroosmotic flow field in packed capillaries can offer significantly superior dispersion characteristics relative to pressure-driven flow.[11–13] The ultimate gain in the performance of an electrokinetically driven mobile phase for capillary electrochromatography (CEC) thus currently attracts tremendous attention, because it is still unclear which factors determine the limits of such an improvement and when the limits actually appear in practice. A study of the transport phenomena must include a careful consideration of the effects of the column walls, the column-to-particle diameter ratio, flow heterogeneity on a macroscopic (column) and a microscopic (pore) level, intraparticle transport characteristics, as well as film mass transfer resistance.

Electroosmotic perfusion phenomena in combination with capillary transport models play an important role in many areas of the physical and life sciences, such as in the dewatering of waste sludge or the removal of contaminants from soil.[14] In CEC, which uses the electrokinetics to drive both the liquid and the (usually charged) solute through fixed particulate beds, an intraparticle convection mechanism for improving mass transfer is largely unexplored. Only a few studies indicate the existence of an intraparticle electroosmotic flow (EOF) and the potential that this effect, together with electrophoretic selectivity, may offer in separation science.[15–21] In simple electrokinetic terms the Helmholtz–Smoluchowski equation implies that the average EOF velocity in a pore segment of the particles is relatively independent of the pore geometry if the characteristic dimension, like the pore radius ($r_{pore}$), is much larger than the thickness of the electrical double layer ($\kappa^{-1}$), namely, $\kappa r_{pore} \gg 1$.[22–25] We then expect a rather flat flow profile over the cross-section of any pore and it also suggests that film mass transfer resistance is negligible in CEC over a wide range of conditions.[26] A particular feature is that average pore velocities can still be significant compared to the typical purely diffusive timescales even when $\kappa r_{pore} \rightarrow 1$ and $r_{pore}$ is only a few nanometers.[22, 23] For thin electrical double layers, these considerations leave the intraparticle tortuosity factor ($\tau_{intra}$) as one of the most critical parameters that determine the extent of electroosmotic perfusive solute transport. $\tau_{intra}$ also reflects the pore connectivity and consequently that fraction of the pore space which transects the particles without dead-end branching and should allow a net EOF to develop.[21]

Herein we provide clear evidence for the existence and enormous impact of an electroosmotic perfusion mechanism in porous media. We studied the performance of pressure-driven flows and EOF through a fixed bed consisting of charged porous particles packed into a capillary by using a pulsed field gradient NMR method as a noninvasive motion-encoding technique that operates (on the millisecond timescale) directly on the nuclear spin of the fluid molecules (for example, $^1H_2O$).[27] Detailed descriptions of this approach concerning its implementation on the capillary dimension and the application to dispersion, flow, and mass-transfer studies in chromatographic media have recently been published.[28, 29] We start with an analysis of the axial dispersion as a function of the particle Péclet number (Pe) for both modes of fluid flow, then complement these data by the selectively measured dynamics of the intraparticle mass transfer, and also address the influence of thermal effects. Our results are finally discussed in regard to the hierarchical design of these particles and thereby achieved correlation of pore interconnectivity in a bidisperse pore network.

The effective axial dispersion coefficient ($D_{ax}$) is obtained from the complex NMR signal $E_{\Delta}(\boldsymbol{q})$ at an observation time ($\Delta$) that is sufficient to allow the complete exchange of fluid molecules between intraparticle and interparticle pore spaces (steady-state) and the development of a Gaussian displacement distribution [Eq. (1)].[27]

$$E_{\Delta}(\boldsymbol{q}) = \exp(i2\pi \boldsymbol{q} \cdot \boldsymbol{u}_{av}\Delta - 4\pi^2 \boldsymbol{q}^2 D_{ax}\Delta) \quad (1)$$

$\boldsymbol{u}_{av}$ is the column cross-sectional averaged velocity and $\boldsymbol{q}$ is a wave vector that encodes fluid motion ($i^2 = -1$). Based on these dispersion coefficients, which include the intraparticle

[*] Dr. U. Tallarek, Dr. H. Van As
Laboratory of Molecular Physics and Wageningen NMR Centre
Department of Biomolecular Sciences, Wageningen University
Dreijenlaan 3, 6703 HA Wageningen (The Netherlands)
Fax: (+31) 317-48-2725
E-mail: ulrich.tallarek@water.mf.wau.nl
Dipl.-Chem. E. Rapp, Prof. Dr. E. Bayer
Forschungsstelle für Nukleinsäure- und Peptidchemie
Institut für Organische Chemie der Universität Tübingen
Auf der Morgenstelle 18, 72076 Tübingen (Germany)

[**] We acknowledge support of this work by a Marie Curie Fellowship (for U.T.) under the Training and Mobility of Researchers Program of the EU (ERBFMBI-CT98-3437) and the European Community activity Wageningen NMR Centre (ERBCHGE-CT95-0066).

  1433-7851/01/4009-1684 $ 17.50+.50/0 

mass transfer kinetics, Figure 1 shows a comparison of the electroosmotic and pressure-driven flows at increasing Pe (this is better known in chromatography as the reduced velocity). The EOF shows an overwhelming enhanced performance over pressure-driven flow, and the regime in which

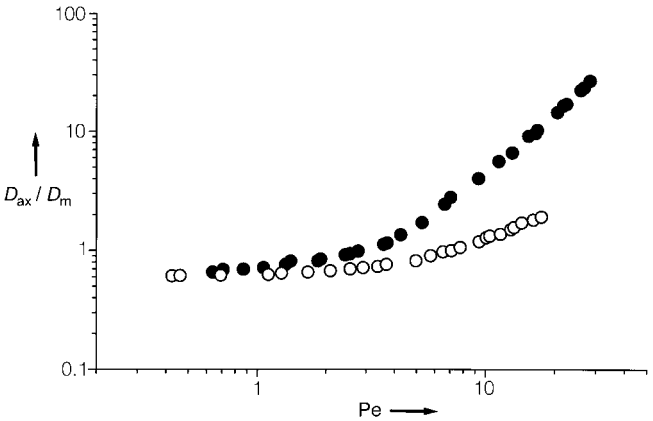


Figure 1. Axial dispersion ($D_{ax}/D_m$) versus the particle Péclet number ($Pe = \boldsymbol{u}_{av} d_p/D_m$) for a 1 mM sodium tetraborate buffer solution at pH 9.13 in a pressure-driven flow (●) and EOF (○). The $^1$H NMR measurements were performed with a special capillary-NMR set up on a 0.5 T electromagnet with open access,[28, 29] and the charged porous particles were packed in a 250 μm i.d. fused-silica capillary. The diffusion coefficient of water is $D_m(25\,^\circ C) = 2.25 \times 10^{-5}\ cm^2 s^{-1}$.

molecular diffusion still controls the dispersion ($D_{ax}/D_m < 1$) extends to much higher Pe. This has already been shown by other research groups.[16, 17, 19] However, it is difficult to relate this improvement quantitatively to any physical mechanism because these data (as in conventional chromatography) are acquired over only a limited range of Pe. This range is hardly sufficient to separate (for example, by a power-law analysis $D_{ax} \propto Pe^{\alpha}$) adequately between dispersion processes originating in the flowing and in the stagnant zones of the packed bed.[30, 31] In pressure-driven flows stochastic velocity fluctuations in the interparticle pore space cause mechanical dispersion which grows linearly with Pe, while regions of zero velocity inside the bed particles and close to their external surface give rise to nonmechanical contributions that grow as $Pe^2$ and $Pe\ln(Pe)$, respectively.[32] In all cases (flow heterogeneity, film mass transfer, and intraparticle diffusion), an electrokinetically driven mobile phase may show a superior performance and $D_{ax}$ only reflects the combined kinetics.

To obtain more direct evidence of the operation of an intraparticle EOF we made a series of NMR measurements within a temporal domain where the exchange of fluid molecules between intraparticle and interparticle pore space environments is not complete over time $\Delta$ (unsteady-state). Then, $E_\Delta(\boldsymbol{q})$ contains discrete contributions from both fluid fractions (stagnant and flowing). By extracting the average number of molecules $A_{intra}(\Delta)$ that are still remaining in the spherical particles at times $\Delta$, this procedure allows a selective study of the intraparticle mass transfer kinetics [Eq. (2)].[28, 33]

$$\frac{A_{intra}(\Delta)}{A_{intra}(0)} = A_{norm}(\Delta) = \frac{6}{\pi^2}\sum_{n=1}^{\infty}\frac{1}{n^2}\exp(-4n^2 B_{intra}\Delta) \qquad (2)$$

In the case of purely diffusive mass-transfer kinetics the rate constant $B_{intra}$ can be further analyzed to calculate the intraparticle diffusion coefficient ($B_{intra} = \pi^2 D_{intra}/d_p^2$) by using the independently measured average particle diameter ($d_p$). Figure 2 compares the exchange kinetics for a constant

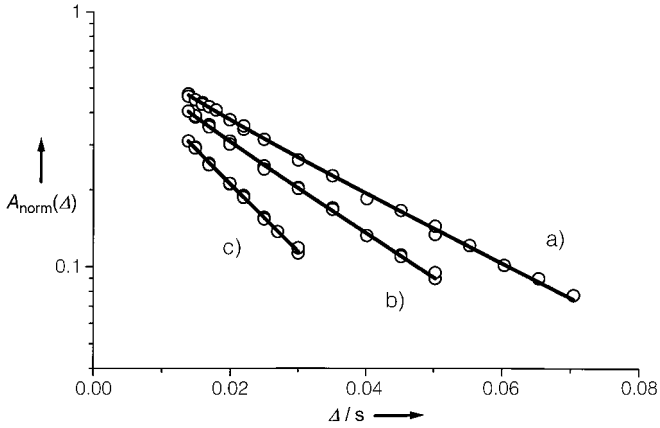


Figure 2. Influence of pressure and potential gradients on stagnant mobile phase mass transfer. The solid lines are best fits of the data to Equation (2) using the pure (a) and effective (b, c) diffusion model. a) Pressure gradient only ($D_{intra} = 1.42 \times 10^{-5}\ cm^2 s^{-1}$). b, c) Effect of a superimposed potential gradient ($E = 47.4\ kV m^{-1}$): b) $D_{ap} = 1.84 \times 10^{-5}\ cm^2 s^{-1}$ (1 mM sodium tetraborate), and c) $D_{ap} = 2.72 \times 10^{-5}\ cm^2 s^{-1}$ (3 mM sodium tetraborate) at pH 9.13.

pressure gradient along the column with those acquired with an additional potential gradient. While the pressure field around the porous particles alone has hardly any measurable influence on diffusion-limited transport ($D_{intra} = 1.42 \times 10^{-5}\ cm^2 s^{-1}$), the electric field enhances significantly the exchange of fluid molecules, and hence increases the intraparticle mass transfer coefficient $B_{intra}$.

This behavior is most probably caused by an electroosmotic perfusion mechanism (and by the existence of an intraparticle electroosmotic flow velocity), but can also be influenced by thermal effects (through the molecular diffusion coefficient $D_m$ at the actual buffer temperature). In the case of perfusion, the apparent diffusivity $D_{ap}$, which is calculated with the simple diffusion model of Equation (2), in fact resembles a combination of an intraparticle EOF and molecular diffusion ($D_{ap} > D_{intra}$). This convection-augmented diffusivity[3–5] is a key parameter in characterizing the improved performance arising from mobile-phase perfusion and is based on the linear driving force approximation.[34–36] Figure 2 shows that $D_{ap}$ even exceeds the molecular diffusivity ($D_m$) of the fluid at higher buffer concentration, and thus leaves the tortuosity-limited regime.

To account for the influence of thermal effects on intraparticle mass transfer we conducted a series of measurements at constant temperature within the capillary while increasing the applied potential gradient (still being the ultimate driving force for any intraparticle EOF). This effect is achieved by a variation of the buffer concentration and adjusting the potential gradient so that the product of electric field strength ($E$) and electric current ($I$) remains constant. The variation of

the buffer concentration at unchanging *EI* (and consequently at the same thermal level) results in an automatic modification of *E*. The results shown in Figure 3 demonstrate

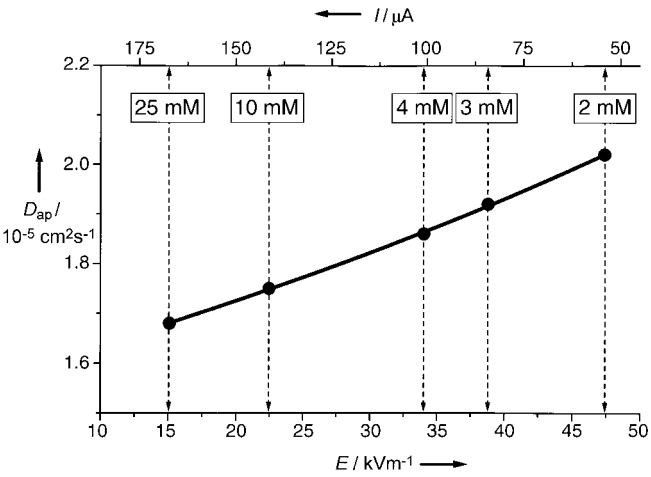


Figure 3. Dependence of the stagnant mobile phase mass transfer kinetics on the electric field strength at a constant level of heat dissipation in the capillary ($EI = 2.54\ \mathrm{W\,m^{-1}}$). While *E* increases, the buffer concentration (and the electrical current *I*) decreases from 25 to 2 mM sodium tetraborate (and *I* from 169 to 54 μA).

a clear dependence of the apparent diffusivity on the electric field strength. This systematic, almost linear, increase in $D_{ap}$ from 1.67 to $2.02 \times 10^{-5}\ \mathrm{cm^2 s^{-1}}$ can only be explained on the basis of a convective transport mechanism. By contrast, a constant diffusivity (independent of *E*) is expected when the intraparticle mass transfer is purely diffusive, that is, only achieved by molecular diffusion at the actual (but constant) buffer temperature. The electroosmotic perfusion will be of considerable importance in the separation of slowly diffusing solutes ($D_m \ll 10^{-5}\ \mathrm{cm^2 s^{-1}}$) and promises intraparticle Péclet numbers well above unity.[21]

To correlate our results with concrete particle characteristics, we now focus on the topology of the intraparticle pore network. These hierarchically structured particles are engineered by clustering inter-adhering microspheres in several steps. The resulting particles consist of two relatively discrete sets of pores, namely, large gigapores[5] (400 – 600 nm, with $d_{pore}/d_p > 10^{-2}$) and macropores (50 – 100 nm).[37] More importantly, this hierarchical design produces an excellent correlation of the interconnectivity between these two sets of pores and minimizes dead-end branching. The gigapores transect the particle as a whole and form the primary basis for intraparticle EOF (Figure 4). The macropores are also large enough to allow an EOF by adjustment of the buffer concentration—within a convenient range—to the actual pore dimensions so that $\kappa r_p \gg 1$. Perfusive solute transport, which in addition utilizes the set of smaller pores, is impossible with pressure-driven flows! As the liquid phase is continuous and incompressible, the volume flow and the radial distribution of velocities in an interconnected pore depend on fluid body forces which originate in all neighboring pores, actually in the medium as a whole. Thus, although the microscopic

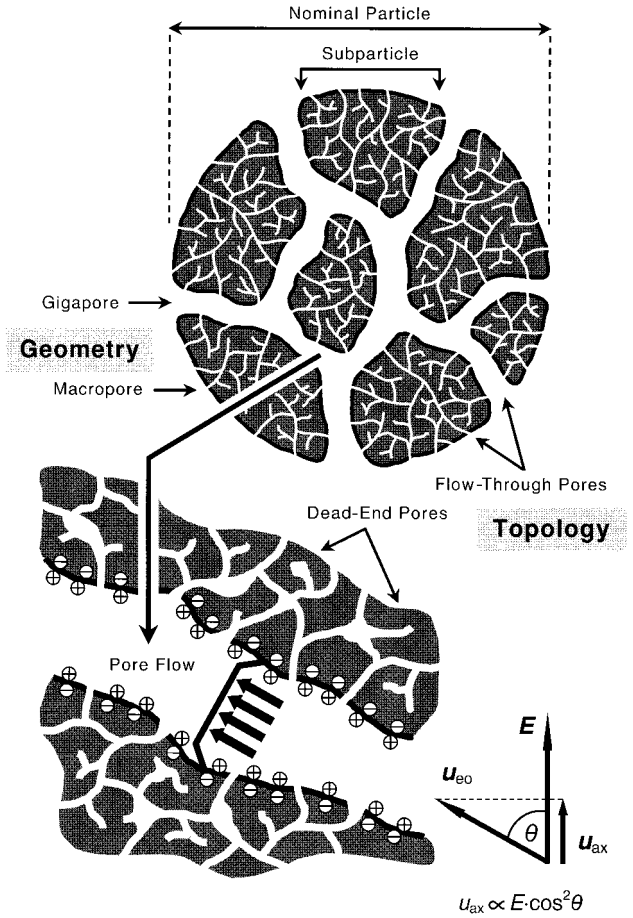


Figure 4. Pore network of a hierarchically structured particle with a bidisperse distribution of pore sizes. In general, the axis of a virtually isolated pore is at an angle $\theta$ to the electric field vector $\boldsymbol{E}$. When $\kappa r_p \gg 1$, the presence of a pluglike EOF with a linear pore velocity ($u_{eo}$) proportional to $E\cos\theta$ is suggested. An unfavorable orientation of pores ($0 < \theta < 90°$) reduces or even prevents ($\theta = 90°$) pore-level EOF in this decoupled single-channel view. In an unconsolidated porous medium, in contrast, all these pores are usually interconnected.

flow profiles then become convex or concave and deviate from a perfect plug-flow behavior, it also means that (viscous) flow through perpendicular pores ($\theta = 90°$) can be achieved. By contrast, no net flow exists in a dead-end pore.

Thus, a more important aspect concerning the intraparticle pore network appears to be the pore interconnectivity rather than the average diameter of the pores. Even for small pores, the buffer concentration—at least within the practical range that can be obtained, but which is still a wide range—can be matched with the pore dimensions, so that $\kappa r_p \gg 1$ (and at least $\kappa r_p > 1$) is guaranteed.

In this context, the tortuosity factor $\tau_{intra}$ relates the steady-state intraparticle diffusion coefficient to the bulk molecular diffusivity ($\tau_{intra} = D_m/D_{intra}$). By using the value for $D_{intra}$ obtained from the diffusion-limited mass-transfer kinetics (Figure 2) we calculate a $\tau_{intra} = 1.58$, which is close to values previously measured for very similar supports.[28] This value suggests a high correlation of pore interconnectivity and the small amount of dead-end pores (see Figure 4) in hierarchically structured media, which is in good agreement with results of numerical studies (although there is no unique

  1433-7851/01/4009-1686 $ 17.50+.50/0 

relation between interconnectivity in a network model and the experimental tortuosity factor).[9, 21, 38, 39]

Our data demonstrate that a significant enhancement in the performance of CEC over capillary HPLC lies in the different dimension of the perfusion mechanism. The intraparticle tortuosity factor $\tau_{intra}$ plays a key role in achieving that goal in both cases, and may also have a sensitive influence on pore migration for charged solutes. Further development in CEC particle technology should focus on the minimum pore size of the through-pore network which still allows a significant intraparticle EOF at decent buffer concentrations, while keeping the surface-to-volume ratio of the pore space attractive for the separation (gigapores, which are used in pressure-driven flows, are not required for electroosmotic perfusion). CEC is easily realized with nanoparticles using hierarchically structured media of micrometer dimension, which leaves molecular diffusion as the ultimate limitation to performance.[40, 41] Thus, the perfusive EOF field translates to an even higher separation efficiency than can currently be achieved in CEC, increased mass sensitivity in on-line coupling schemes (such as nano-ESI-MS), and the possibility of using pressurized CEC for higher analysis speed and flow stability, without significant increase in dispersion.

Received: October 30, 2000 [Z16012]


[1] N. B. Afeyan, N. F. Gordon, I. Mazsaroff, L. Varady, S. P. Fulton, Y. B. Yang, F. E. Regnier, *J. Chromatogr.* **1990**, *519*, 1 – 29.
[2] A. I. Liapis, M. A. McCoy, *J. Chromatogr.* **1992**, *599*, 87 – 104.
[3] A. E. Rodrigues, J. C. Lopes, Z. P. Lu, J. M. Loureiro, M. M. Dias, *J. Chromatogr.* **1992**, *590*, 93 – 100.
[4] G. Carta, M. E. Gregory, D. J. Kirwan, H. A. Massaldi, *Sep. Technol.* **1992**, *2*, 62 – 72.
[5] D. D. Frey, E. Schweinheim, Cs. Horváth, *Biotechnol. Prog.* **1993**, *9*, 273 – 284.
[6] R. H. Davis, H. A. Stone, *Chem. Eng. Sci.* **1993**, *48*, 3993 – 4005.
[7] D. H. Reeder, A. M. Clausen, M. J. Annen, P. W. Carr, M. C. Flickinger, A. V. McCormick, *J. Colloid Interface Sci.* **1996**, *184*, 328 – 330.
[8] P.-E. Gustavsson, P.-O. Larsson, *J. Chromatogr. A* **1996**, *734*, 231 – 240.
[9] J. J. Meyers, A. I. Liapis, *J. Chromatogr. A* **1998**, *827*, 197 – 213.
[10] J. F. Pfeiffer, J. C. Chen, J. T. Hsu, *Am. Inst. Chem. Eng. J.* **1996**, *42*, 932 – 939.
[11] M. M. Dittmann, K. Wienand, F. Bek, G. P. Rozing, *LC-GC* **1995**, *13*, 800 – 814.
[12] A. L. Crego, A. González, M. L. Marina, *Crit. Rev. Anal. Chem.* **1996**, *26*, 261 – 304.
[13] L. A. Colón, K. J. Reynolds, R. Alicea-Maldonado, A. M. Fermier, *Electrophoresis* **1997**, *18*, 2162 – 2174.
[14] R. F. Probstein, *Physicochemical Hydrodynamics: An Introduction*, Wiley, New York, **1994**.
[15] E. Venema, J. C. Kraak, H. Poppe, R. Tijssen, *J. Chromatogr. A* **1999**, *837*, 3 – 15.
[16] R. Stol, W. Th. Kok, H. Poppe, *J. Chromatogr. A* **1999**, *853*, 45 – 54.
[17] E. Wen, R. Asiaie, Cs. Horváth, *J. Chromatogr. A* **1999**, *855*, 349 – 366.
[18] A. I. Liapis, B. A. Grimes, *J. Chromatogr. A* **2000**, *877*, 181 – 215.
[19] P. T. Vallano, V. T. Remcho, *Anal. Chem.* **2000**, *72*, 4255 – 4265.
[20] R. Stol, H. Poppe, W. Th. Kok, *J. Chromatogr. A* **2000**, *887*, 199 – 208.
[21] B. A. Grimes, J. J. Meyers, A. I. Liapis, *J. Chromatogr. A* **2000**, *890*, 61 – 72.
[22] C. L. Rice, R. Whitehead, *J. Phys. Chem.* **1965**, *69*, 4017 – 4024.
[23] R. J. Gross, J. F. Osterle, *J. Chem. Phys.* **1968**, *49*, 228 – 234.
[24] Q.-H. Wan, *Anal. Chem.* **1997**, *69*, 361 – 363.
[25] S. Arulanandam, D. Li, *Colloids Surf. A* **2000**, *161*, 89 – 102.
[26] A. I. Liapis, B. A. Grimes, *J. Colloid Interface Sci.* **2000**, *229*, 540 – 543.
[27] P. T. Callaghan, J. Stepišnik, *Adv. Magn. Opt. Reson.* **1996**, *19*, 325 – 388.
[28] U. Tallarek, F. J. Vergeldt, H. Van As, *J. Phys. Chem. B* **1999**, *103*, 7654 – 7664.
[29] U. Tallarek, E. Rapp, T. Scheenen, E. Bayer, H. Van As, *Anal. Chem.* **2000**, *72*, 2292 – 2301.
[30] M. Sahimi, *Applications of Percolation Theory*, Taylor & Francis, London, **1994**.
[31] J. H. Knox, *J. Chromatogr. A* **1999**, *831*, 3 – 15.
[32] D. L. Koch, J. F. Brady, *J. Fluid Mech.* **1985**, *154*, 399 – 427.
[33] J. Crank, *The Mathematics of Diffusion*, Clarendon, Oxford, **1956**.
[34] A. E. Rodrigues, B. J. Ahn, A. Zoulalian, *Am. Inst. Chem. Eng. J.* **1982**, *28*, 541 – 546.
[35] A. Leitão, A. Rodrigues, *Chem. Eng. J.* **1995**, *60*, 81 – 87.
[36] G. Carta, *Chem. Eng. Sci.* **1995**, *50*, 887 – 889.
[37] D. Whitney, M. McCoy, N. Gordon, N. Afeyan, *J. Chromatogr. A* **1998**, *807*, 165 – 184.
[38] J. H. Petropoulos, J. K. Petrou, A. I. Liapis, *Ind. Eng. Chem. Res.* **1991**, *30*, 1281 – 1289.
[39] M. P. Hollewand, L. F. Gladden, *Chem. Eng. Sci.* **1992**, *47*, 2757 – 2762.
[40] J. H. Knox, *Chromatographia* **1988**, *26*, 329 – 337.
[41] K. K. Unger, S. Lüdtke, M. Grün, *LC-GC Int.* **1999**, *12*, 870 – 874.


# First, Atropo-Enantioselective Total Synthesis of the Axially Chiral Phenylanthraquinone Natural Products Knipholone and 6′-*O*-Methylknipholone**

Gerhard Bringmann* and Dirk Menche

*Dedicated to Professor Wolfgang Kiefer on the occasion of his 60th birthday*

Among the more than one hundred anthraquinone natural products with biaryl axes,[1] phenylanthraquinones,[2–4] like knipholone (**1a**)[2] and 6′-*O*-methylknipholone (**1b**),[3] occupy a special position: Since they are constitutionally unsymmetric, they are most likely formed biosynthetically by a directed, enzymatic biaryl coupling and not merely by a "chemical" dimerization of the corresponding monoanthraquinones. A further hint at such an enzymatic origin of **1a** and **1b** is the fact that they are optically active and are thus axially chiral. First isolated by Dagne and Steglich in 1984,[2] knipholone (**1a**) and related phenylanthrachinones have been found in numerous African plant species of the genera *Bulbine*, *Bulbinella*, and *Kniphofia* (all Asphodelaceae),[4] which are widely used in folk medicine.[2, 5]

[*] Prof. Dr. G. Bringmann, Dipl.-Chem. D. Menche
Institut für Organische Chemie
Universität Würzburg
Am Hubland, 97074 Würzburg (Germany)
Fax: (+49) 931-888-4755
E-mail: bringman@chemie.uni-wuerzburg.de

[**] Novel Concepts in Directed Biaryl Synthesis, Part 93. This work was supported by the Deutsche Forschungsgemeinschaft (grant: SFB 347) and by the Fonds der Chemischen Industrie. We thank Prof. B. M. Abegaz und Dr. M. Bezabih for an authentic sample of 6′-*O*-methylknipholone and for valuable discussions. We thank J. Kraus for helpful suggestions and V. Barthel for technical support. Part 92: G. Bringmann, J. Hinrichs, K. Peters, E.-M. Peters, *J. Org. Chem.* **2001**, *66*, 629 – 632.